Radio Pulsars and EoS

Manjari Bagchi

ICTS & WVU

30 May, 2013

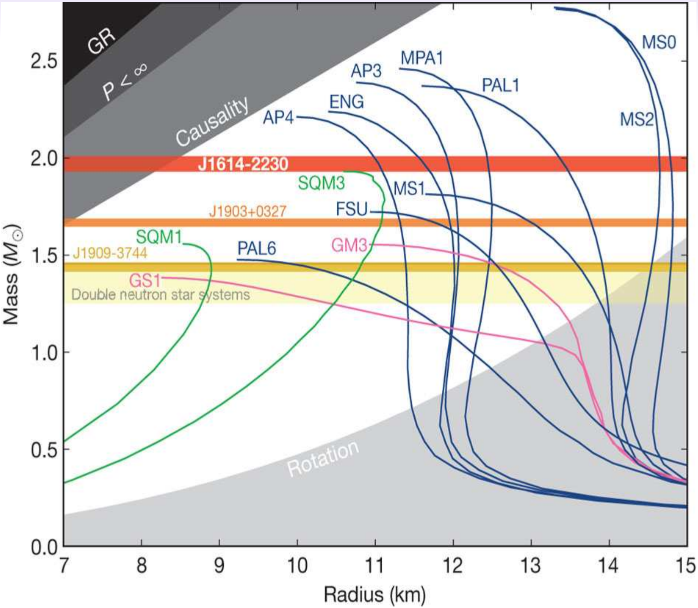
GR
P < ∞
Causality
J1614-2230
J1903+0327
J1909-3744
Double neutron star systems
Rotation
AP4
ENG
AP3
MPA1
PAL1
MS0
MS2
MS1
SQM3
FSU
SQM1
PAL6
GM3
GS1
Mass ($M_\odot$)
Radius (km)

A Massive Pulsar in a Compact Relativistic Binary

SCIENCE VOL 340 26 APRIL 2013

John Antoniadis,[1*] Paulo C. C. Freire,[1] Norbert Wex,[1] Thomas M. Tauris,[2,1] Ryan S. Lynch,[3] Marten H. van Kerkwijk,[4] Michael Kramer,[1,5] Cees Bassa,[5] Vik S. Dhillon,[6] Thomas Driebe,[7] Jason W. T. Hessels,[8,9] Victoria M. Kaspi,[3] Vladislav I. Kondratiev,[8,10] Norbert Langer,[2] Thomas R. Marsh,[11] Maura A. McLaughlin,[12] Timothy T. Pennucci,[13] Scott M. Ransom,[14] Ingrid H. Stairs,[15] Joeri van Leeuwen,[8,9] Joris P. W. Verbiest,[1] David G. Whelan[13]

Many physically motivated extensions to general relativity (GR) predict substantial deviations in the properties of spacetime surrounding massive neutron stars. We report the measurement of a 2.01 ± 0.04 solar mass ($M_\odot$) pulsar in a 2.46-hour orbit with a 0.172 ± 0.003 $M_\odot$ white dwarf. The high pulsar mass and the compact orbit make this system a sensitive laboratory of a previously untested strong-field gravity regime. Thus far, the observed orbital decay agrees with GR, supporting its validity even for the extreme conditions present in the system.

Dense Matter Equations of State

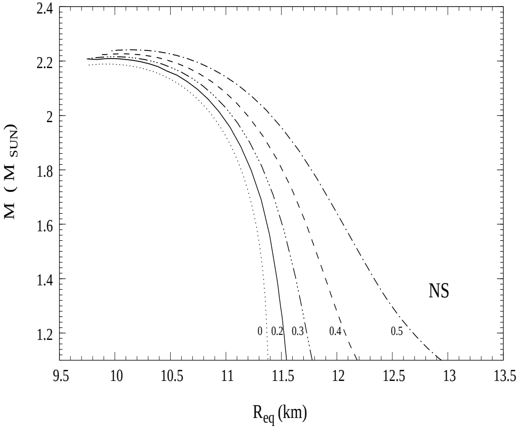

RNS Code: *http://www.gravity.phys.uwm.edu/rns/*

Ω in units of $10^4\ \mathrm{s}^{-1}$

NS mass measurements: 2012, ApJ, 757, 55

ON THE MASS DISTRIBUTION AND BIRTH MASSES OF NEUTRON STARS

Feryal Özel[1], Dimitrios Psaltis[1], Ramesh Narayan[2], Antonio Santos Villarreal[1]

[1]Department of Astronomy, University of Arizona, 933 N. Cherry Ave., Tucson, AZ 85721 and
[2] Harvard-Smithsonian Center for Astrophysics, 60 Garden St., Cambridge, MA 02138

Draft version September 10, 2012

ABSTRACT

We investigate the distribution of neutron star masses in different populations of binaries, employing Bayesian statistical techniques. In particular, we explore the differences in neutron star masses between sources that have experienced distinct evolutionary paths and accretion episodes. We find that the distribution of neutron star masses in non-recycled eclipsing high-mass binaries as well as of slow pulsars, which are all believed to be near their birth masses, has a mean of 1.28 $M_\odot$ and a dispersion of 0.24 $M_\odot$. These values are consistent with expectations for neutron star formation in core-collapse supernovae. On the other hand, double neutron stars, which are also believed to be near their birth masses, have a much narrower mass distribution, peaking at 1.33 $M_\odot$ but with a dispersion of only 0.05 $M_\odot$. Such a small dispersion cannot easily be understood and perhaps points to a particular and rare formation channel. The mass distribution of neutron stars that have been recycled has a mean of 1.48 $M_\odot$ and a dispersion of 0.2 $M_\odot$, consistent with the expectation that they have experienced extended mass accretion episodes. The fact that only a very small fraction of recycled neutron stars in the inferred distribution have masses that exceed $\sim 2\,M_\odot$ suggests that only a few of these neutron stars cross the mass threshold to form low mass black holes.

DNS	Masses	e	P_{orb}	$\sin i$	P_{s1}	μ_α	μ_δ	$\dot{\omega}_{obs}$	Refs.
	$M_\odot$		days		s	mas yr^{-1}	mas yr^{-1}	deg yr^{-1}	
J0737-3039	1.3381 (m_1) 1.2489 (m_2)	0.08778	0.10225	0.999	0.02270 2.77346	-3.3	2.6	16.89947	R1
J1518+4904	$0.72^{+0.51}_{-0.58}$ $2.00^{+0.58}_{-0.51}$	0.24948	8.63401	–	0.04093	-0.67	-8.53	0.01137	R2
B1534+12	1.33 1.35	0.27368	0.42074	0.975	0.03790	1.34	-25.05	1.75580	R3
J1753-2240†	– > 0.49	0.30358	13.63757	–	0.09514	–	–	–	R4
J1756-2251	1.312 1.258	0.18057	0.31963	0.95	0.02846	-0.7	–	2.58254	R5
J1807-2500B† (NGC 6544B)	1.3655 1.2064	0.74703	9.95667	0.9956	0.00419	–	–	0.01834	R6
J1811-1736	$1.11^{+0.53}_{-0.15}$ $1.62^{+0.22}_{-0.55}$	0.82801	18.77917	–	0.10418	–	–	0.0090	R7
B1820-11†	–	0.79461	357.76199	–	0.27983	~ 300	~ 200	0.00007	R8
J1829+2456	< 1.38 $1.22 - 1.38$	0.13914	1.17603	–	0.04101	–	–	0.28	R9
J1906+0746†	1.248 1.365	0.0853	0.16599	–	0.14407	–	–	7.57	R10
B1913+16	1.4398 1.3886	0.61713	0.323	0.71*	0.05903	-1.43	-0.70	4.2266	R11
B2127+11C (M15C)	1.358 1.354	0.6814	0.33528	–	0.03053	-1.3	-3.6	4.4644	R12

NS mass measurements for radio pulsars:

$R = m_A/m_B = a_1 \sin i / a_2 \sin i$
$m_A = 1.3381(7), m_B = 1.2489(7)$

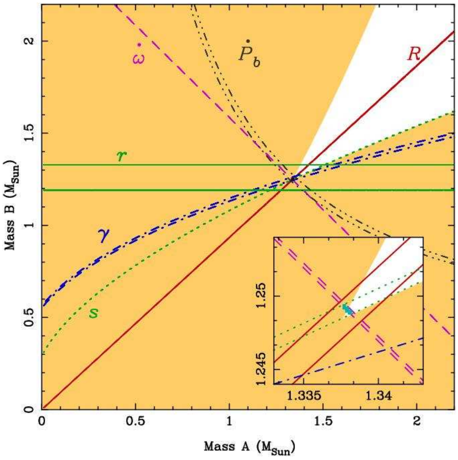

Double Pulsar J0737-3039 (A,B): Lyne *et al.* 2004, Science, 303, 1153
Kramer *et al.* 2006, Science, 314, 97

PK parameters:

$$T_\odot = \frac{GM_\odot}{c^3} = 4.92540 \ \mu\mathrm{s}$$

$$\dot{\omega} = 3T_\odot^{2/3} \left(\frac{P_b}{2\pi}\right)^{-5/3} \frac{1}{1-e^2} \, (m_p + m_c)^{2/3}$$

$$\gamma = T_\odot^{2/3} \left(\frac{P_b}{2\pi}\right)^{1/3} e \, \frac{m_c(m_p + 2m_c)}{(m_p + m_c)^{4/3}}$$

$$r = T_\odot m_c$$

$$s = \sin i = T_\odot^{-1/3} \left(\frac{P_b}{2\pi}\right)^{-2/3} x \, \frac{(m_p + m_c)^{2/3}}{m_c}$$

$$\dot{P}_b = -\frac{192\pi}{5} T_\odot^{5/3} \left(\frac{P_b}{2\pi}\right)^{-5/3} f(e) \frac{m_p m_c}{(m_p + m_c)^{1/3}}$$

$$f(e) = \frac{1 + (73/24)e^2 + (37/96)e^4}{(1-e^2)^7/2}$$

Keplerian Parameters (mass function):

$$\frac{(m_c \sin i)^3}{(m_p + m_c)^2} = \frac{4\pi^2}{G} \, \frac{(a_p \sin i)^3}{P_b^2}$$

We need both M, R to constrain EoS.

R from LMXBs: J. M. Lattimer & M. Prakash, 2007, Phys. Rep, 442, 109; S. Bhattacharyya, 2010, AdSpR, 45, 949

Radio astronomers can (in principle) determine I.

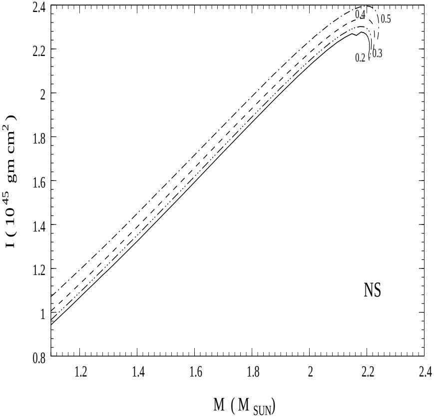

RNS Code: *http://www.gravity.phys.uwm.edu/rns/*

Moment of Inertia Determination:

Damour & Schafer, 1988, Nuovo Cimento B, 101, 127

$$\dot{\omega} \;=\; \dot{\omega}_{1PN} + \dot{\omega}_{2PN} + \dot{\omega}_{\mathrm{SO}} \;=\; \frac{3\beta_0^2\, n}{1-e^2}\left[1 + f_0\beta_0^2 - (g_{s1}\beta_{s1} + g_{s2}\beta_{s2})\beta_0\right]$$

$$\beta_0 \;=\; \frac{(GMn)^{1/3}}{c}, \quad \beta_{sa} \;=\; \frac{cI_a}{Gm_a^2}\cdot\frac{2\pi}{P_{s,a}}$$

$$f_0 \;=\; \frac{1}{1-e^2}\left(\frac{39}{4}x_1^2 + \frac{27}{4}x_2^2 + 15x_1x_2\right) - \left(\frac{13}{4}x_1^2 + \frac{1}{4}x_2^2 + \frac{13}{3}x_1x_2\right)$$

$$x_1 \;=\; m_1/M, \quad x_2 \;=\; m_2/M, \quad M = m_1 + m_2$$

Moment of Inertia Determination:

Damour & Schafer, 1988, Nuovo Cimento B, 101, 127

$$\dot{\omega} \;=\; \dot{\omega}_{1PN} + \dot{\omega}_{2PN} + \dot{\omega}_{\rm SO} \;=\; \frac{3\beta_0^2\; n}{1-e^2}\left[1 + f_0\beta_0^2 - g_{s1}\beta_{s1}\beta_0\right]$$

$$\beta_0 \;=\; \frac{(GMn)^{1/3}}{c}, \quad \beta_{sa} \;=\; \frac{cI_1}{Gm_1^2}\cdot\frac{2\pi}{P_{s,1}}$$

$$f_0 \;=\; \frac{1}{1-e^2}\left(\frac{39}{4}x_1^2 + \frac{27}{4}x_2^2 + 15x_1x_2\right) - \left(\frac{13}{4}x_1^2 + \frac{1}{4}x_2^2 + \frac{13}{3}x_1x_2\right)$$

$$x_1 \;=\; m_1/M, \quad x_2 \;=\; m_2/M, \quad M = m_1 + m_2$$

$f_0\beta_0^2 = 2.6\times10^{-5}$ (max) for PSR J0737-3039A
$\quad = 0.15\times10^{-5}$ (min) for PSR J1518+4904

Best estimate of $\dot{\omega}$ (PSR J0737-3039A/B): 16.89947 ± 0.00068 deg yr^{-1}

Moment of Inertia Determination:

$$g_{s1} = \frac{x_1\,(4x_1 + 3x_2)}{6(1-e^2)^{1/2}\sin^2 i} \times \left[(3\,\sin^2 i - 1)\ \mathbf{k}\ + \cos i\ \mathbf{h}\ \right].\ \mathbf{s_1}$$

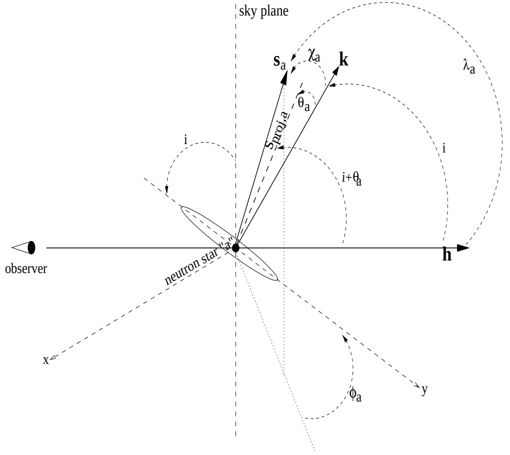

Moment of Inertia Determination:

$$g_{s1} = \frac{x_1\,(4x_1 + 3x_2)}{6(1-e^2)^{1/2}\sin^2 i} \times \left[(3\,\sin^2 i - 1)\,\mathbf{k} + \cos i\,\mathbf{h}\right].\,\mathbf{s_1}$$

For $\mathbf{s_1} \parallel (3\,\sin^2 i - 1)\,\mathbf{k} + \cos\, i\,\mathbf{h}$:

$$g_{s1,\,max} = \left[3 + \frac{1}{\sin^2\, i}\right]^{1/2} \frac{x_1\,(4x_1 + 3x_2)}{6(1-e^2)^{1/2}}$$

For $\mathbf{s_1} \parallel \mathbf{k}$:

$$g_{s1,\,\parallel} = \frac{x_1\,(4x_1 + 3x_{bh})}{3(1-e^2)^{1/2}}$$

$g_{s1,\,max}$ differs from $g_{s1,\,\parallel}$ by the factor $\frac{1}{2}\left[3 + \frac{1}{\sin^2\, i}\right]^{1/2}$, which lies between $1.7 - 1.0$ for i in the range of $20^\circ - 90^\circ$.

Sub-millisecond pulsars might help:

J.M. Lattimer, M. Prakash / Physics Reports 442 (2007) 109–165 117

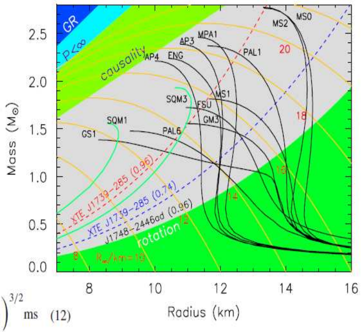

$$P_{\min} \simeq (0.96 \pm 0.03)\left(\frac{M_\odot}{M_{\rm sph}}\right)^{1/2}\left(\frac{R_{\rm sph}}{10\,{\rm km}}\right)^{3/2} {\rm ms} \quad (12)$$

Fig. 2. Mass-radius trajectories for typical EOSs (see [6] for notation) are shown as black curves. Green curves (SQM1, SQM3) are self-bound quark stars. Orange lines are contours of radiation radius, $R_\infty = R/\sqrt{1-2GM/Rc^2}$. The dark blue region is excluded by the GR constraint $R > 2GM/c^2$, the light blue region is excluded by the finite pressure constraint $R > (9/4)GM/c^2$, and the green region is excluded by causality, $R > 2.9GM/c^2$. The light green region shows the region $R > R_{\max}$ excluded by the 716 Hz pulsar J1748-2446ad using Eq. (12). The upper red dashed curve is the corresponding rotational limit for the 1122 Hz X-ray source XTE J1739-285 ; the lower blue dashed curve is the rogorous causal limit using the coefficient 0.74 ms in Eq. (12).

Binary Radio Pulsars: Detectability

Johnston & Kulkarni, 1991, ApJ, 368, 504

Bagchi, Lorimer, Wolfe, 2013, MNRAS, 432, 1303

$$S_{obs} = {\gamma_1}^2 S_{intr}$$

Acceleration search can recover this power (partially): γ_2

$$S_{obs} = {\gamma_2}^2 S_{intr}$$

Binary Radio Pulsars: Detectability

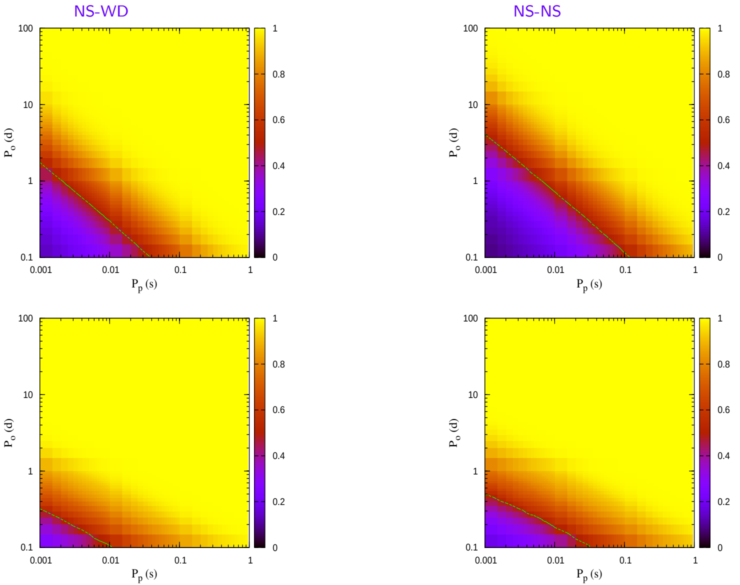

$e = 0.5,\ T_{obs} = 1000$ s